Proceedings of the 11th International Conference on Fluid Flow, Heat and Mass Transfer (FFHMT 2024)
Niagara Falls, Canada – June 16-18, 2024
Paper No. 009
DOI: 10.11159/ffhmt24.009

Drag Reduction Effects Associated with Streamwise Triangular Riblet (STR) Microstructures

William Gordon[1,2], O. Remus Tutunea-Fatan[1,2], Evgueni Bordatchev[2,1]
[1]University of Western Ontario
1151 Richmond St, London, Canada wgordon5@westerneng.ca;
rtutunea@eng.uwo.ca
[2]National Research Council of Canada
800 Collip Circle, London, Canada evgueni.bordatchev@nrc-cnrc.gc.ca

Abstract - Significant research efforts were recently made in studying hydrodynamics of a turbulent water flow over surfaces structured with various micro-scale features. Past studies have demonstrated drag reduction, self-cleaning, and fouling-resistant effects of streamwise triangular riblets (STR), also known as sawtooth riblets, and other riblet designs. The goal of this study was to numerically simulate and parametrically analyse the effect of included angle (α) of STRs on potential drag reduction effects. The CFD simulations performed within the scope of the current study were focused on the effect of design parameters on turbulent flow hydrodynamics as well as their effect on drag reduction performance. The analysis considered several different values of the included angle, namely α = 15°, 30°, and 60° at multiple flow velocities. The flow conditions – particularly the turbulent structures formed around the riblets – have been analysed in detail and have been compared with published data. CFD simulations were run by means of the LES WALE model encompassing a prism and hexahedral mesh. The examination of the turbulent flow patterns near riblet tips and valleys revealed that the flow exhibits characteristics consistent with those published in the past for 60° STR. Moreover, as α decreases, the range of nondimensional riblet spacing (S+) exhibiting drag reducing effects reduces while the range of Reynolds number increases. The smaller value of the analysed included angle seemed to be associated with maximum drag reduction (~10%) for smaller S+ values. The results of this study are expected to open new avenues towards the development, optimization, and control of advanced hydro- and aerodynamic functional surfaces.

***Keywords*:** Drag Reduction, Sawtooth Riblets, Streamwise Triangular Riblets (STR), CFD, LES WALE, Turbulence

1. Introduction

Surfaces with micro-scale riblets could exhibit novel and advanced fluid dynamic properties compared to their flat counterparts. There are numerous applications that rely on the control and alteration of fluid dynamics in proximity to surfaces that possess textures or structures. Although this not a recent research area, a large number of unknowns continue to exist. Along these lines, the current study will attempt to determine the effect of the included angle of streamwise triangular riblets - also referred to as sawtooth riblets (STR) – on drag reduction. The wide-range analysis of the impact of STR structures on drag reduction was inspired by shark skin and its microscopic surface structures that are characterized by semicircular grooves running parallel to flow direction and grouped together in small scales called dermal denticle [1, 2].

Past search efforts were focused on the analysis of the attributes and potential uses of the STR structures. For instance, extensive investigations have delved into the understanding of the effect of a staggered arrangement of 3D riblets on drag reduction [3]. Other studies attempted to uncover the correlation between debris accumulation or riblet tip wear and their effect on riblet performance [4]. Furthermore, significant efforts have been made to analyse the effect of different riblet types (STR, blade riblets, asymmetrical triangular riblets, etc.) on flow manipulation [5]. Some studies relied on experiments to investigate the effect of compliance in the material the riblets were affixed to, in an attempt to mimic the compliance of actual sharkskin [6]. Anti-fouling and self-cleaning are other interesting properties of STR structures that have also been

computationally and experimentally examined [7]. Large-scale simulations studying the overall effects of riblets on a Stratos 716 X business jet have been conducted [8]. Along the same lines, tests on an Airbus 320 airplane exhibiting STR structures of 60° showed a 2% reduction in fuel usage [9]. Despite having a substantial knowledge base to start from, further research on optimizing these riblets and comprehending their properties is essential and therefore conducting extensive parametric studies represents an effective approach to achieve this goal.

To address this, the main objective of the present study was to analyse the effect of varying the included angle of the riblets on the drag reductive properties, the expectation being that this knowledge will further facilitate the understanding of the mechanism of passive drag reduction. As part of this effort, upcoming sections will provide details on comparisons performed between CFD simulations and experimental data.

2. Numerical Simulation and Experimental Methodologies

2.1. Numerical Simulation Methodology

Two different series of simulations were completed in this study and they will be detailed further. In the first series, the velocity of the fluid was varied over the featured surface in order to vary the $S+$ value. However, because of the increased Reynolds numbers associated with the increased velocity, a higher level of turbulence is more likely in some of the cases. To account for this variation, a second series of simulations were performed. The second set of simulations was completed by relying on a new model for each simulation. In this approach, the riblet spacing could be varied in order to manipulate the $S+$ value without increasing or decreasing the fluid velocity associated with initial flow conditions.

The first step of the numerical solution was the creation of the swept prism and hexahedral grid in ANSYS. The mesh type and parameters were based on past studies [10]. The element size for features and top surface were set at 35 μ m and in the large central area at 750 μ m. Split lines were used to have more control over the cell growth rather than a simple inflation rate (Fig. 1). The drastically larger element size in the central section was used in order to reduce the number of cells and thus reduce the computation time. The element size in this section is much less important than near the top and featured surfaces since there is significantly less turbulence to be modelled in this region [11]. All simulations used identical meshes and the same mesh parameters when the domains were different.

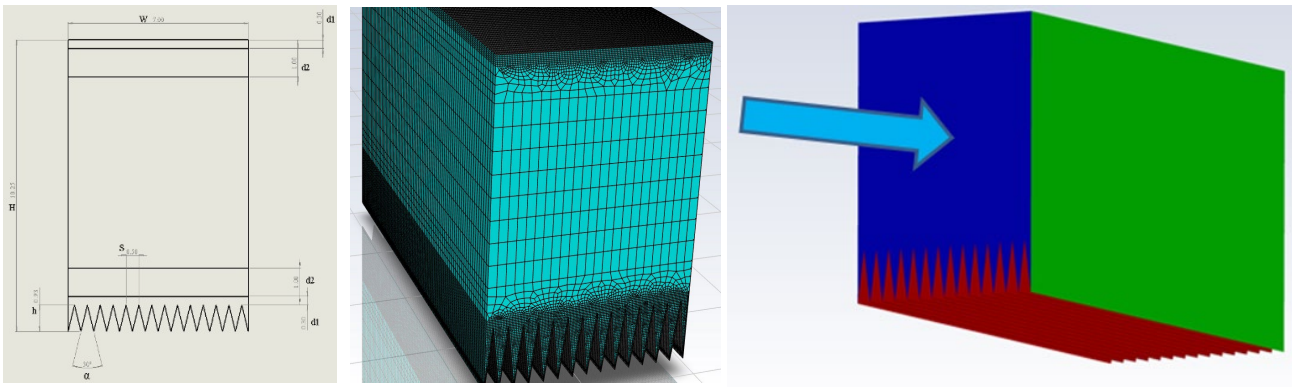

Fig. 1: Parameters of the geometric domain (left), mesh sample (center), flow direction (right).

In FLUENT, the viscous model was set as LES WALE since this is one of the most extensive turbulent flow models. This model requires significantly more cells than other models such as the k-ε model as such LES is more computationally demanding. To reduce the computation time, all simulations were started off as steady state RANS (standard k-ε). This was selected such that the initial data for the transient simulations has a much closer resemblance to the actual established velocity. This initial data has turbulent fluctuations initialized in order to "trip" the flow into turbulence. The inlet, outlet, left, and right walls were defined as periodic interfaces in order to simulate an infinitely long and wide domain. Under the periodic boundary conditions, the cases varying the riblet spacing are characterized by a specified mass flow rate of Q = 0.04 kg/s that changes as a function of the inlet area. The mass flow rate was set only in the x-direction and the initial pressure gradient is set as 0 Pa/m. The top and featured surfaces are set up with a no-slip wall boundary condition. The time step of these simulations was initially defined as the smallest element size/average velocity and then varied

throughout the simulation. After running the simulation for around 10,000 iterations, the number of iterations per time step required is noted. Depending on what this number is, the time step can either be increased, decreased, or remained the same.

2.2. Experimental Performance Evaluation Methodology

The experiments used to validate the numerical results relied on an apparatus capable to measure the pressure gradient caused by drag changes produced by surface structures (Fig. 2). A D5100 pressure transducer from TE Connectivity was used to measure the pressure gradient. This sensor has a total error of ±103.4Pa. The data was read by a LabVIEW program, then was uploaded to a Matlab program that was used to take a time average of each measurement. Additionally, the Matlab program was used to linearly offset the data based on two zero measurements taken at the beginning and the end of each experiment in an attempt to account for slight variations in the atmospheric pressure.

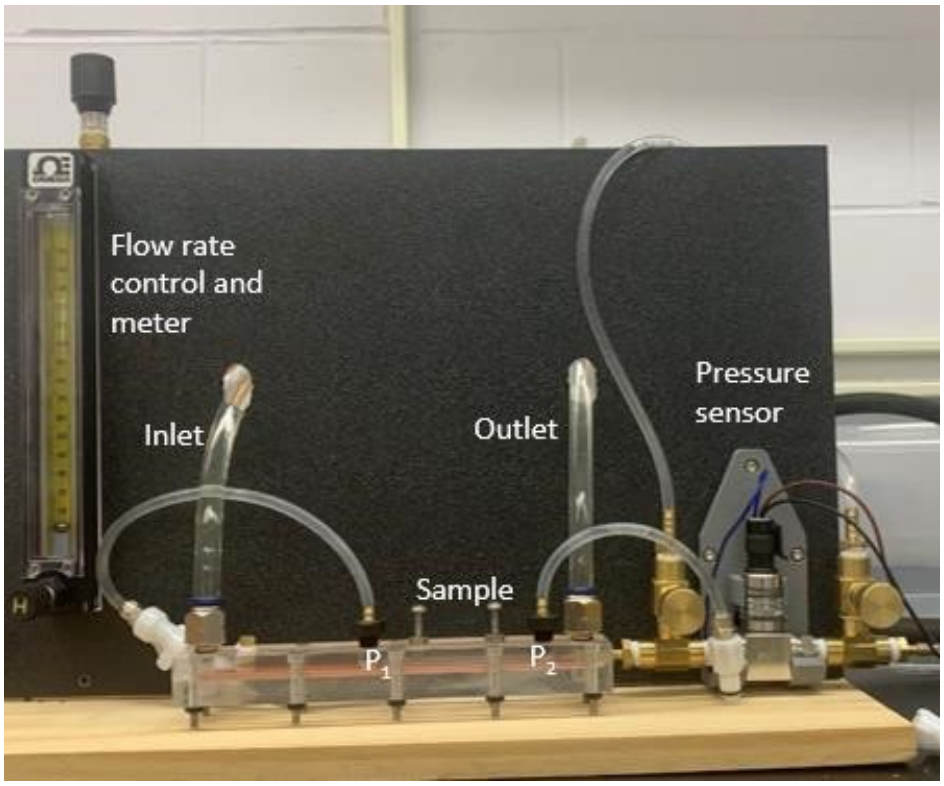

Fig. 2: Experimental setup.

Four samples were manufactured from acrylic, each characterized by these angles: 15°, 30°, 60° and flat with no features, respectively. The riblet spacing was chosen at 235 μm. The features were machined by means of single point diamond cutting tool installed on a five-axis micromachining center. The geometric parameters selected were in agreement both with past simulations as well as the experimental device to be used.

3. Results and Discussion

3.1. The Effect of Flow Velocity on Drag

The results of the numerical simulations performed for variable STR angles and mass flow rates facilitate several critical observations (Fig. 3). More specifically, as α decreases, so does the Reynolds number at which peak reduction occurs. This has important implications – for instance – in applications where lower velocities desirable in a sense that they should be characterized by STRs with lower angles. These results also suggest that riblets with a shallower angles should be placed near the front of a vessel whereas – as Reynolds number increases towards the rear of the ship – the ones with an increasingly larger angle should be placed towards the rear. Moreover, these preliminary results also seem to imply that the range of *Re* at which drag reduction occurs shrinks as α increases. Nonetheless, this idea requires further investigation since the number of data points used in this study was low.

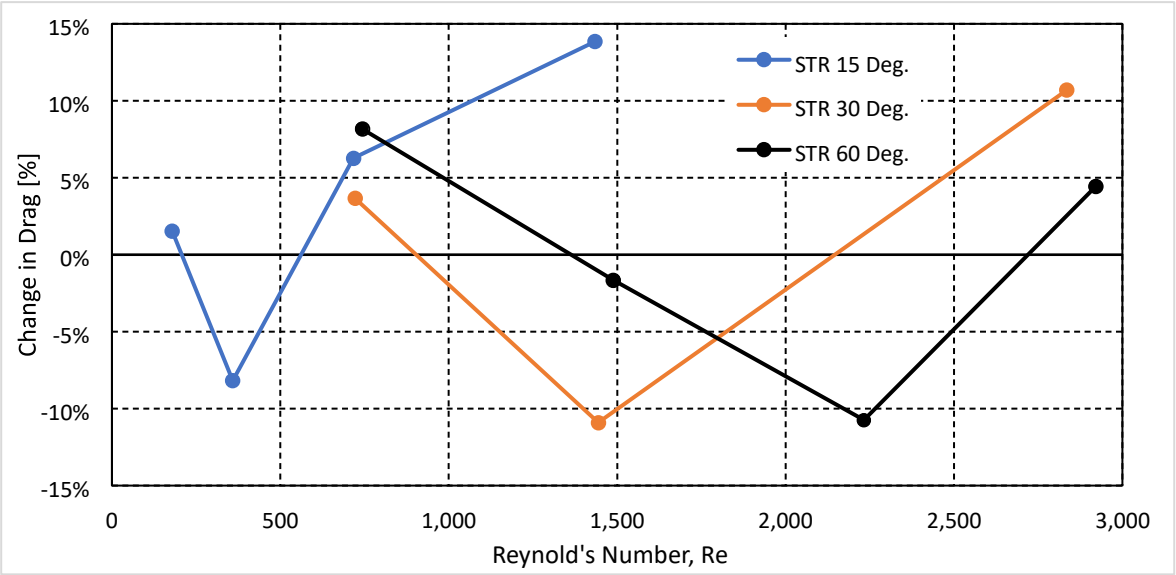

Fig. 3: Correlation between mass flow rate, drag reduction and STR angle.

3.2. The Effect of Riblet Spacing on Drag

The numerical results associated with variable riblet spacings are presented in Fig 4. According to them, when α = 15° the peak drag reduction occurs around $S+ = 9$ rather than the expected $S+ = 10 – 20$. However, a previous study [5] did indicate that as α decreases same happens to the $S+$ value at which peak drag reduction happens. This trend is also observed in the results associated with α = 30° and α = 60° cases. Something worth mentioning about these cases is represented by the decreased area in drag reductive region of the curve (as α decreases). A similar comment was made by Bechert et. al. [6] and this might explain the reduced drag reductive "window" visible in Fig. 7. If this observation is will be experimentally validated, it could have important implications on the design of drag reductive riblets for different applications in a sense that a riblet with a larger included angle can provide drag reduction for a larger window of velocities, or riblet spacing.

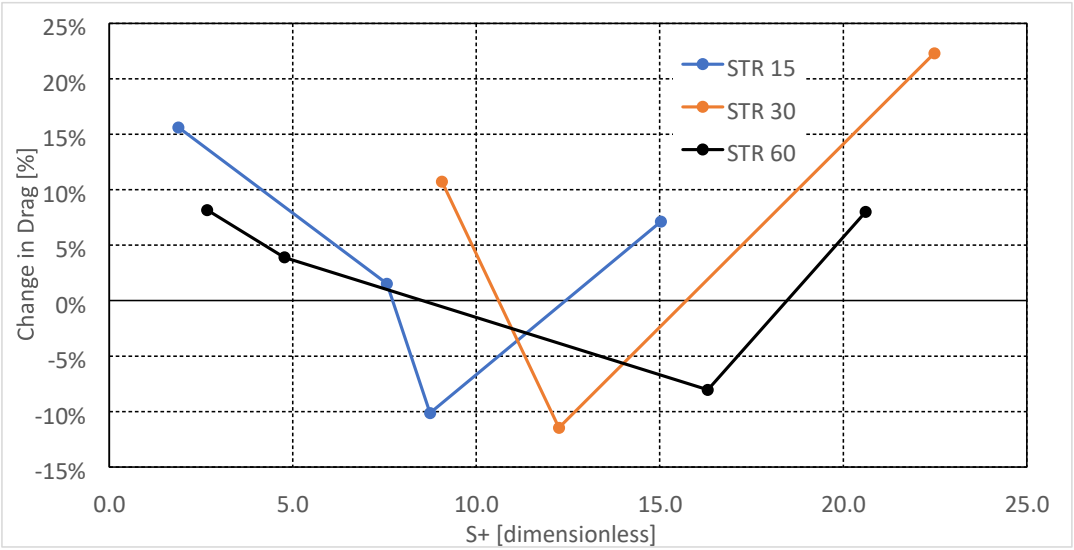

Fig. 4: Dependence between drag reduction and $S+$ in case of a constant mass flow rate.

Two main hypotheses were proposed by Martin and Bhushan [2] to explain the mechanisms through which these riblets can reduce the skin friction drag. According to one of them, drag reduction is a consequence of the reduction in the velocity

of fluctuations in the spanwise direction. The second possibility is that the geometry of the structures prevents the formation of streamwise vortices within the riblet valleys. In other words, the turbulences are being lifted and pushed away from the surface.

The numerical results obtained in this study seem to be aligned with both theories proposed so far. More specifically, the velocity-RMSE fields – computed using the velocity fluctuations, see Eq. (1) – require data sampling for time statistics to be monitored during simulations. The results of this analysis are presented in Fig. 5 for the α = 15° case. Interestingly, the increase in w-RMSE between the drag decreasing and drag increasing cases occurs just above the riblet peaks. On the other hand, a factor of roughly 3.75 affects the peak w-RMSE value for α = 15° drag decreasing/increasing scenarios. These increased velocity fluctuations cause an increase in drag through an increased turbulence at the riblet peaks.

$$\text{w-RMSE} = \sqrt{\frac{\sum_i^N (w_i - \overline{w_i})^2}{N}} \tag{1}$$

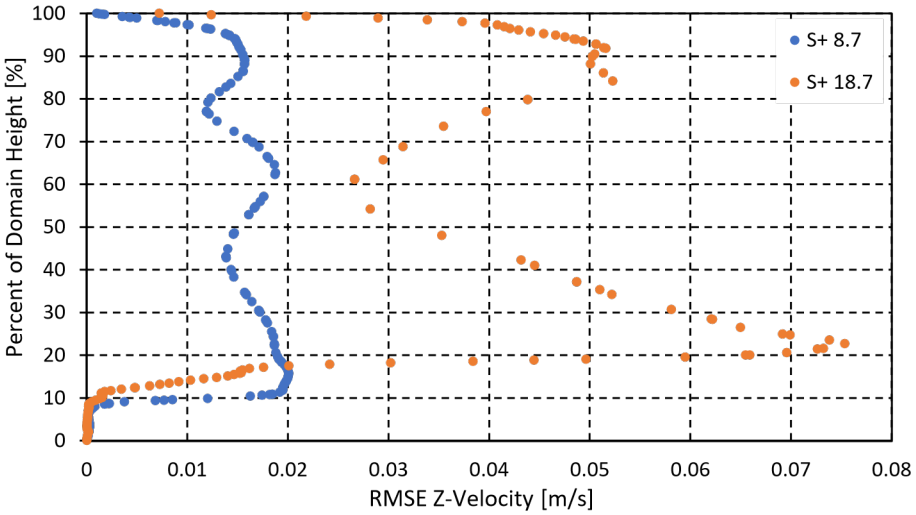

Fig. 5: RMSE-z velocity as a function of domain height for α = 15° when drag is decreasing ($S+$ = 8.7) or increasing ($S+$ = 18.7).

The theory of reduction in streamwise eddies is illustrated in Fig. 6 that depicts velocity vectors in the plane perpendicular to the flow. The colour scale of all plots is 1.08e-7 – 0.73 m/s. Graphical representations of the velocity fields determined in both drag increasing and decreasing scenarios suggest that drag increasing is associated with a higher velocity above the riblets than its decreasing counterpart. On the other hand, the drag increasing cases are characterized by a streamwise vorticity that travels further down on the riblet valley than in the drag decreasing case. Similar observations were also made in [1] such that it can be asserted that drag decreasing is correlated with less intense streamwise vortices in the riblet valley and near the riblet peaks.

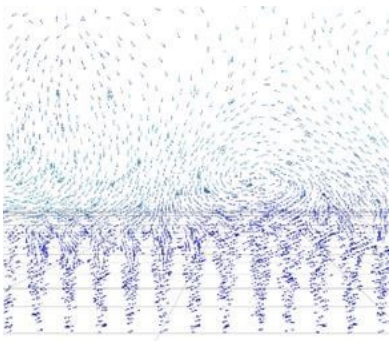

a) drag decreasing ($S+$ = 8.7)

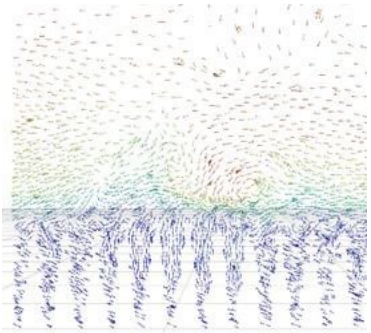

b) drag increasing ($S+$ = 18.7)

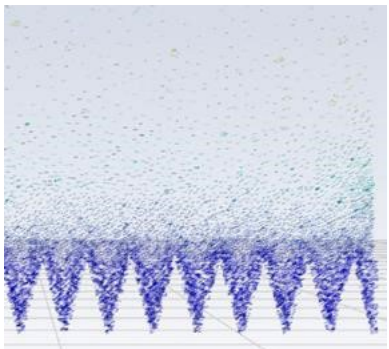

c) 30° drag decreasing ($S+$ = 10.2)

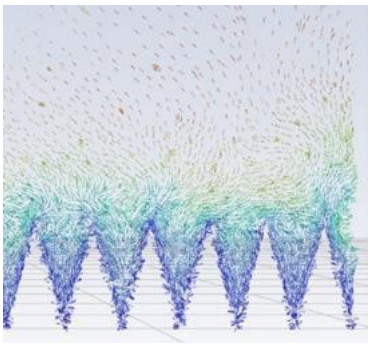

d) 30° drag increasing ($S+$ = 15.5)

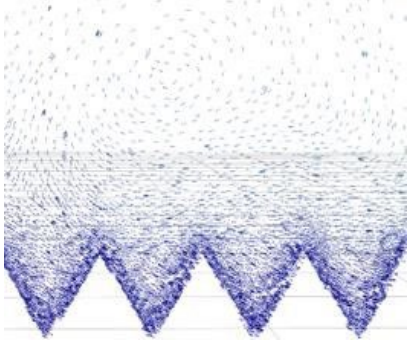

e) 60° drag decreasing ($S+$ = 11.8)

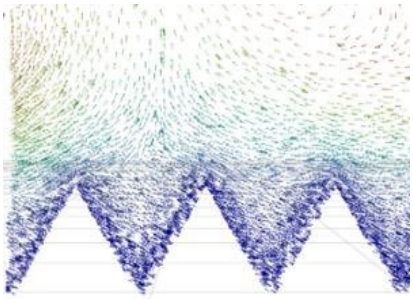

f) 60° drag increasing ($S+$ = 20.7)

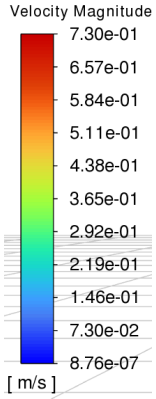

g) Scale

Fig. 6: Velocity vectors in a center plane perpendicular to the flow direction for: a-b) α = 15°, c-d) α = 30°, e-f) α = 60°, and g) is the scale.

An alternate method that allows a more facile visualization of the same physical phenomenon involves z-vorticity contours (Fig. 7). These plots reveal with more clarity the larger and violent turbulent that ensue in drag increasing cases above the riblet peaks. Furthermore, the plots also illustrate vorticity's trend to travel deeper into the riblet valleys for steep STR angles. This phenomenon leads to increased area of contact between surface structures and streamwise vortices ultimately leading to drag increases. The scale of contours presented in Fig. 7 is 0-118 [1/s]. Colourless areas exhibit vorticities above the maximum value of the scale.

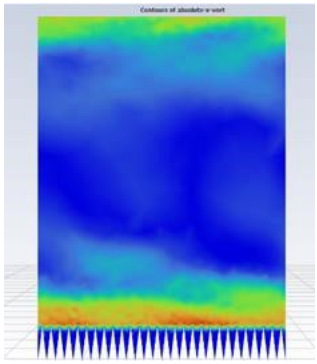

a) drag decreasing ($S+ = 8.7$)

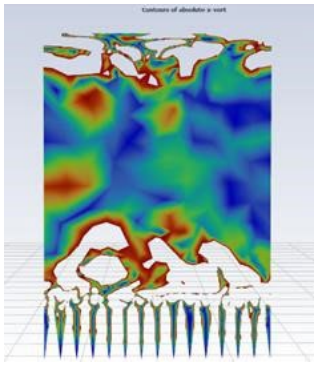

b) drag increasing ($S+ = 18.7$)

Fig. 7: Contours of streamwise vorticity for: a) $\alpha = 15°$ drag decreasing ($S+ = 8.7$) and b) $\alpha = 15°$ drag increasing ($S+ = 18.7$) cases.

3.3. Experimental Results

Unfortunately, the experimental tests performed so far were inconclusive since their results did not match the insight provided by the numerical data yielded both from this study and previous ones. While the root cause of this misalignment between numerical and experimental data is still being examined, it is possible that the flat surfaces perpendicular to the flow direction that are present before the sample (Fig. 8) are leading to a wake in the riblet valleys that might have an effect on the subsequent vorticities created in the proximity of the STR structures. Furthermore, since the same flat surface is also present at the rear of the sample, it is possible that a back pressure is created as the fluid in the riblet valleys suddenly collides with this surface (once the sample has ended).

Nonetheless, while the absence of correlation between numerical and experimental data cannot be explained at this time, it is worth to mention that the correlation was in fact near perfect for a different type of structure that did not have, however, the forward and backwards facing steps that are characteristic to the STR samples tested in this study. In other words, it is believed that the misalignment between the numerical and experimental data is caused by certain geometric features present in the sample and not by the apparatus itself. To counteract the effect of these features, alternate testing methods will be developed in the future.

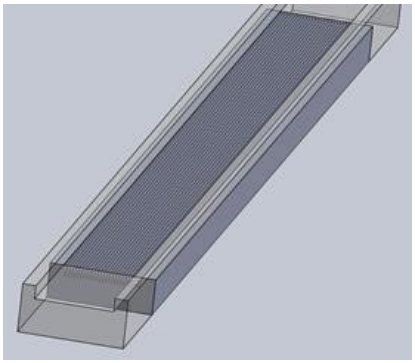

Fig. 8: Water conduit outlining the flat areas located pre and post-sample.

4. Conclusions

While the experimental results obtained so far were inconclusive/unaligned with those obtained from simulations, the numerical ones align well with the previously reported ones. If the redesigned experimental setup will enable the validation of the numerical data, the strength of the previously-made comments/observations on the reduced drag reductive window of Reynolds number and $S+$ value for riblets with smaller values of α will be significantly enhanced. Also important, both Reynolds number and $S+$ value associated with maximum drag reduction appear to be lower for riblets characterized by smaller angles. Nonetheless, experimental validation is still required before any decisive statements can be made on any of these topics.

Acknowledgements

The work presented in this study is the result of the collaboration between Western University (London, Ontario, Canada) and National Research Council of Canada (London, Ontario, Canada). Partial financial support was also provided by Natural Sciences and Engineering Research Council (NSERC) of Canada. The significant technical support provided by Mr. Benjamin Hamilton, a PhD candidate in the same research team is gratefully acknowledged.

References

[1] S.-J. Lee and S.-H. Lee, "Flow Field Analysis of a turbulent boundary layer over a Riblet surface," *Experiments in Fluids*, vol. 30, no. 2, pp. 153–166, 2001.

[2] S. Martin and B. Bhushan, "Fluid Flow Analysis of a shark-inspired microstructure," *Journal of Fluid Mechanics*, vol. 756, pp. 5–29, 2014.

[3] B. R. Smith, P. Yagle and P. D. McClure, "Computational Simulation of Staggered 3-D Riblets for Skin Friction Drag Reduction," *AIAA SCITECH 2023 Forum*, 2023

[4] P. A. Leitl, C. Feichtinger, G. Schatzdorfer and A. Flanschger, "Measurement of riblet defects and their impact on performance," *AIAA SCITECH 2021 Forum*, 2021

[5] S. Endrikat, D. Modesti, R. García-Mayoral, N. Hutchins, D. Chung, "Influence of riblet shapes on the occurrence of Kelvin–Helmholtz Rollers," *Journal of Fluid Mechanics*, vol. 913, 2021.

[6] D. W. Bechert, M. Bruse, W. Hage, J. G. Van Der Hoeven, G. Hoppe, "Experiments on drag-reducing surfaces and their optimization with an adjustable geometry," *Journal of Fluid Mechanics*, vol. 338, pp. 59–87, 1997.

[7] H. O. Benschop, A. J. Guerin, A. Brinkmann, M. L. Dale, A. A. Finnie, W.-P. Breugem, A. S. Clare, D. Stübing, C. Price, K. J. Reynolds, "Drag-reducing riblets with fouling-release properties: Development and testing," *Biofouling*, vol. 34, no. 5, pp. 532–544, 2018.

[8] P. A. Leitl, J. Smoker, M. L. Garcia de Albeniz and A. Flanschger ""Numerical and experimental investigation of different Riblet layouts on a Stratos 716 X business jet," *AIAA SCITECH 2023 Forum*, 2023

[9] R. García-Mayoral and J. Jiménez, "Drag reduction by Riblets," *Philosophical Transactions of the Royal Society A: Mathematical, Physical and Engineering Sciences*, vol. 369, no. 1940, pp. 1412–1427, 2011

[10] F. Yifeng, Y. Chengqing, B. Xiuqin, L. Tao, "Study on drag reduction performance of antifouling ribbed surfaces," *Journal of Ship Production and Design*, vol. 34, no. 1, pp. 32–41, 2018. [11] Ansys® *Meshing User's Guide, Release 13.0, Help System*, ANSYS, Inc.